# Finite Element Analysis of Cardiac Electric Activity in a Monodomain system for a class of Ionic models

B.V.Rathish Kumar[1] and Meena Pargaei[2]

[1,2]*Indian Institute of Technology Kanpur, Department of Mathematics and Statistics, India*

**Abstract**

In this study we derive the Finite element apriori error estimate for the Monodomain cardiac electric model in conjunction with the generic form for a class of nonlinear ionic models. The analysis establishes a $o(h^2 + k)$ space-time convergence. Further the computational realization of the same for different reduced ionic test models is presented.Also, the coupled parabolic PDE and ODE system modeling the Cardiac Electric Activity in a Monodomain system representation of cardiac tissue with different Ionic models (at cell level) viz. FitzHugh-Nagumo model(FHNM), Roger-McCulloch model(RMM), Aliev-Panfilov model(APM) and Mitchell-Schaeffer model(MSM) are numerically analyzed by Galerkin Finite Element method in space and Backward Euler method in time. Simulations are done using FreeFem++ open source and the evolution pattern of the solution has been investigated. MSM and RMM model are, unconditionally stable with respect to applied stimulus and initial state, although other models are conditionally stable.

*Keywords:* Cardiac Electric Activity, Apriori Estimate, Finite Element Method, ODE-PDE system.

## 1. Introduction

Cardiac arrhythmia (CA) is known to be one of leading causes of death in the world. CA is known to occur due to irregular propagation of electric potential in heart. Cardio electrophysiology is a branch of medical science that deals with the cardiac electric activity (CEA). CEA is responsible for expansion and contraction of heart muscles which in turn regulates the blood pumping and blood receiving activity of heart. Mathematical modelling and numerical simulation is a viable means to study CEA. Feasibility of such a study depends on the availability of appropriate mathematical models and apt numerical schemes to tackle such models. These mathematical models and numerical tools can serve as diagnostic tools.

There are various CEA models at the cell and tissue level. These models consist of coupled ODE-PDE system. The ODEs describe the electrical activity at the cellular level while the PDEs describe the potential flow across the network of cells. Bidomain model [4] is one of these models which is described by a system of two degenerate parabolic reaction-diffusion equations to trace the intracellular, extracellular and transmembrane potentials in cardiac tissue and it is coupled with a system of ODEs to trace the ionic currents flowing through the cellular membrane. Monodomain model [4] is a simplified form of the bidomain model and it consists a parabolic reaction diffusion equation which describes the trace of transmembrane potential across the heart muscle and a system of ODEs dealing with activity at the cell level.

Few attempts have been made to solve the coupled nonlinear degenerate parabolic PDEs together with stiff nonlinear ODEs modelling the ionic and gating variables numerically by Finite difference method, Finite element method etc. [14, 15, 4, 6]. These studies are essentially focused on either Bidomain model or Monodomain model with a specific ionic model. For theoretical investigation of spatial and temporal scales few reduced ionic models such as FithzHugh Nagumo(FHN) model, Roger-MCculloch(RM) model, Panfilov model and Mithchell-Schaeffer(MS) model have been proposed. Though these reduced model overlook sub-cellular processes, they have been found to be effective in the 1-D studies as presented in [7]. Now it is essential to workout a comparative assessment of effectiveness of these models for closing the tissue level description of

*Email address:* meenap@iitk.ac.in (B.V.Rathish Kumar[1] and Meena Pargaei[2])

[1]Corresponding author :Indian Institute of Technology Kanpur, Department of Mathematics and Statistics, F520, India

CEA. Such a multi-dimensional model comparative study is currently not available in literature and hence the investigation is focused on this study.

In this paper we solve the Monodomain model with various reduced ionic models using linear finite elements to discretize in space and backward Euler method for time discretization. Simulation is done using FreeFem++. The paper is organized as follows: section (2) introduces the tissue and cell level CEA models. In section (3) we derive the apriori error estimate for the semi-discrete and fullly discrete both. Section (4) deals with the numerical methodology and Finite element discretization. Details on the numerical simulation with discussion is presented in section (5). Finally the conclusions are drawn in section (6).

## 2. Introduction to general ideas of cardiac electrical models

Since a long time experimental studies of cardiac electrical activity has been supplemented by computational models of transmembrane potential propagation. Quantitative description of transmembrane potential can be provided by these models and have more importance because they are useful to test and come up with the conclusions that are difficult to test experimentally.

Cardiac tissue contains excitable cells. When the voltage reaches above it threshold value, $Na^+$- voltage gated ion channels open and a rapid membrane deplolarization takes place which generates an action potential.This action potential is responsible for the flow of the current within the tissue. Due to this current flow, voltage-gated $Na^+$ channels of the neighboring electrically connected cells also open and this results in the generation of the action potential through the tissue.

Electrical coupling of the cardiac cells is by the gap junctions, which are organized into fibers and which in turn are organized into sheets. More than one hundred models of cardiac cells are presented in literature, which are called as Ionic models, consisting of the stiff system of ODEs, which varies both in their complexity and in the level of detail. Since cardiac tissue is a network of cells, to describe the electrical activity in the whole heart, tissue level space-time model (PDE model) has to be coupled with cell level model (i.e. ionic models (ODEs model)). Bidomain model and Monodomain model are two such tissue level models and FHN, RM, Panfilov and MS are popular cell level models and these models are briefly discussed below.

### *2.1. Bidomain Model*

Cardiac tissue is considered as the overlapping of the intra and extracellular continuous domains such that each point in the intracellular myocardium is also in the extracellular and the two domains are connected with continuous cellular membrane. Bidomain model is the characterization of such cardiac tissue, consists of a set of mathematical equations which describe the propagation of intra and extracellular electric potentials in cardiac tissue.

Let $J_i$ and $J_e$ are the intra and extracellular conductivity tensors respectively. This conductivity comes into picture due to the fiber structure of the cardiac tissue (see Fig. 1). This fiber structure also influences the flow of electric currents. There are three basic directions for the conductivity (i) along the direction of fiber, (ii) orthogonal to fiber direction, but in the plane of cardiac tissue sheet, (iii) orthogonal to the cadiac tissue sheet. Fiber conductivity changes with direction.

Mathematical equations in terms of the intra and extracellular electric potentials, transmembrane potential and gating variable, $u^i, u^e, u$ and $w$ respectively is given by

$$C^m \frac{\partial u}{\partial t} - div(J^i(x)\nabla u^i) + I^{ion}(u,w) = I^i_{app} \qquad \text{in} \quad \Omega \times (0,T), \tag{1}$$

$$C^m \frac{\partial u}{\partial t} + div(J^e(x)\nabla u^e) + I^{ion}(u,w) = I^e_{app} \qquad \text{in} \quad \Omega \times (0,T), \tag{2}$$

$$\frac{\partial w}{\partial t} - g(u,w) = 0 \qquad \text{in} \quad \Omega \times (0,T), \tag{3}$$

$$n^t J^{i,e}(x)\nabla u^{i,e} = 0, \qquad \text{on} \quad \partial\Omega \times (0,T), \tag{4}$$

$$u(x,0) = u_0(x), \qquad w(x,0) = w_0(x) \quad \text{in} \quad \Omega. \tag{5}$$

where,

$$J^s(x) = \sigma_l{}^s b_l(x) b_l{}^t(x) + \sigma_t{}^s b_t(x) b_t{}^t(x) + \sigma_n{}^s b_n(x) b_n{}^t(x), \qquad s = \{i, e\}$$

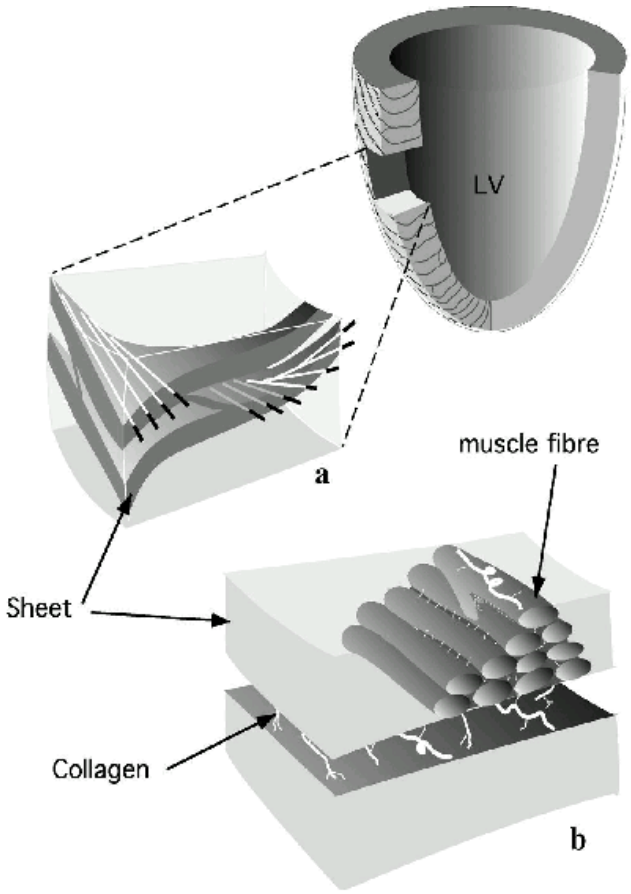


Figure 1: The cross section of muscle fiber in the left ventricle(LV) [12].

with $b_l(x), b_t(x), b_n(x)$ are orthonormal vectors corresponding to the three basic directions, (i) along the direction of fiber, (ii) orthogonal to fiber direction but in the plane of cardiac tissue sheet, (iii) orthogonal to the cardiac tissue sheet, respectively.

If ${\sigma_n}^s = {\sigma_t}^s$,

$J^s(x) = {\sigma_t}^s I + ({\sigma_l}^s - {\sigma_t}^s) b_l(x) {b_l}^t(x), s = \{i, e\}$.

$I^i_{app}, I^e_{app}$ are the applied current in the intra and extracellular domains respectively. $I^{ion}(u, w)$ and $G(u, w)$ are given by ionic models at the cell level, which will be described later.

The compatibility condition for the system is

$$\int_\Omega I^i_{app} = \int_\Omega I^e_{app}.$$

The numerical simulation of the bidomain model with realistic data is time consuming and costly. To reduce this cost many efforts have been made. The monodomain model, simplified version of the bidomain model, is used to calculate the action potential at low cost.

*2.2. Monodomain Model*

The primary assumption for deducing the simplified bidomain model is that the ratio of the conductivity tensors in the intra and extracellular domain is constant, i.e. $J^i/J^e = l(say)$, then the bidomain model reduces to monodomain model [4] which is given by

$$C_m \frac{\partial u}{\partial t} - div(J(x)\nabla v) + I^{ion}(u,w) = I_{app} \qquad \text{in} \quad \Omega \times (0,T), \tag{6}$$

$$\frac{\partial w}{\partial t} - g(u,w) = 0 \qquad \text{in} \quad \Omega \times (0,T), \tag{7}$$

$$n^t J(x)\nabla u = 0 \qquad \text{on} \qquad \partial\Omega \times (0,T), \tag{8}$$

$$u(x,0) = u_0(x), \qquad w(x,0) = w_0(x) \quad \text{in} \quad \Omega, \tag{9}$$

where,

$$J(x) = \sigma_t I + (\sigma_l - \sigma_t) b_l(x) {b_l}^t(x) \quad with \quad \sigma_{l,t,n} = \frac{l\sigma^i_{l,t,n}}{1+l}.$$

There are various papers which deal with the comparison of the bidomain and monodomain model in various expect. In [11], they compared the two models on a small slab of cardiac tissue. They compared the models on the basis of activation time,recovery time and the measurement of APD and reported them to be in good agreement. Again in [10], potentials resulting from the repolarization and depolarization for the bidomain model of human heart is compared with the results of the monodomain model. They found that the difference between the results of bidomain and monodomain models are extremely small.

So, from the above observed results, it can be stated that monodomain model is good enough to produce the action potential results.

*2.3. Ionic Models*

Hodgkin and Huxley in 1952 gave the first mathematical model that describes accurately the action potential waveform. They won the Nobel prize also in Medicine in 1963. In this model they describe the action potential of a nerve cell for squid gaint axon. Therefore, the model is directly not related to study about the heart, but behaves as a good example of cell modeling.

The basic cell model for action potential ($u$) propagation, as accepted by physiologists, is given by the ODE:

$$C^m \frac{du}{dt} = -I^{ion} + I_{app},$$

where $C^m$ is the capacitance, $I^{ion}$ is the ionic currents and $I_{app}$ is the applied stimulus.

The ionic current $I^{ion}$ for the Hodgkin-Huxely model (HHM) is given as the sum of the three currents,

$$I^{ion} = I^{Na} + I^K + I^L,$$

where

$$\begin{aligned} I^{Na} &= G^{Na} m^3 h (u - u^{Na}) \\ I^K &= G^K n^4 (u - u^K) \\ I^L &= G^L (u - u^L), \end{aligned}$$

where $G^{Na}, G^K, G^L$ are the conductances for each current. $u^{Na}, u^K, u^L$ are the equilibrium potentials for the three currents. $m, h, n$ are gate variables described by equations

$$\frac{dw}{dt} = \alpha_w(u)(1-w) - \beta_w(u)w,$$

for $w = m, h, n$.

For large spatial and temporal investigation of any phenomena, various reduced ionic models have been described only to provide the action potential at low cost. These are called the two variable model or the reduced ionic model. The two variables are the transmembrane potential ($u$) and the gating variable ($w$) also called excitation variable and recovery variable respectively. Some of the reduced ionic models are briefly discussed below.

- FitzHugh Nagumo Model(FHNM) [2]

  Hodgkin-Huxely equations are complex. Various simplification have been done which show quantitatively behavior similar to HHM. FHN is an example of such simplified system which is given by

$$\begin{aligned} I^{ion} &= -ku(u-a)(u-1) - w, \\ g(u,w) &= \epsilon(u - \gamma w). \end{aligned}$$

- Roger-McCulloch Model(RMM) [3]

  In 1994, Roger and McCulloch modified the FHN model in such a way that it is more close of cardiac electrical behavior. The action potential in FHN model shows hyperpolarization when $u$ is close to 0 and $w$ is elevated. But the hyperpolarization is not the characterstic of cardiac action potential. This hyperpolarization is eliminated by modifying the last term in $I^{ion}$,

$$\begin{aligned} I^{ion} &= -ku(u-a)(u-1) - uw, \\ g(u,w) &= \epsilon(u - \gamma w). \end{aligned}$$

- Aliev-Panfilov model(APM) [1]

  Aliev and Panfilov made another modification in the FHN ionic model which reproduces the restitution property of cardiac tissue as well as represents the shape of the action potential. This model can be used in whole heart modelling also,

$$\begin{aligned} I^{ion} &= -ku(u-a)(u-1) - uw, \\ g(u,w) &= \epsilon'(-ku(u-1-a) - w), \quad \text{where } \epsilon' = \epsilon_0 + \mu_1 w/(u+\mu_2). \end{aligned}$$

- Mitchell-Schaeffer model(MSM) [5]

  This model includes only inward and outward current. It contains four time constants, for the four phases of cardiac action potential; Initial, plateau, decay and recovery.

$$\begin{aligned} I^{ion} &= -\frac{w}{\tau_{in}}u^2(u-1) - \frac{u}{\tau_{out}}, \\ g(u,w) &= \begin{cases} \frac{1-w}{\tau_{open}} & u \le u_{gate}, \\ \frac{-w}{\tau_{close}} & u > u_{gate}. \end{cases} \end{aligned}$$

**Remark:** For the existence and uniqueness results of the monodoamin system, we refer to [6].

## 3. Apriori error estimate for the semi-discrete problem

Let $\Omega$ be a plane convex domain with smooth boundary and consider the problem (6-8).

Assume that $D(x)$ is symmetric and uniformly positive definite, i.e. there exist $\alpha > 0$ such that $\forall x \in R^3, \forall \xi \in R^3$, $\xi^T D(x)\xi \ge \alpha |\ \xi\ |^2$.

Introducing the inner product $(\begin{bmatrix}\alpha_1 & \alpha_2\end{bmatrix}, \begin{bmatrix}\beta_1 & \beta_2\end{bmatrix})_X := (\alpha_1, \beta_1) + (\alpha_2, \beta_2)$, and the associated norm $\|\cdot\|_X$, where $(\cdot,\cdot)$ is the standard $L^2$- inner product.

Let $\mathbf{u} = \begin{bmatrix}u & w\end{bmatrix}^t$, $G = \begin{bmatrix}\nabla & 0 \\ 0 & 0\end{bmatrix}$, $G\mathbf{u} = G\begin{bmatrix}u \\ w\end{bmatrix} = \begin{bmatrix}\nabla u \\ 0\end{bmatrix}$ So,the weak form of the problem becomes;

Find $u \in H^1(\Omega) \times L^2(\Omega)$ such that

$$(u_t, \psi)_X + (DG\mathbf{u}, G\psi)_X = (F(\mathbf{u}), \psi)_X, \tag{10}$$

where, $F(\mathbf{u}) = \begin{bmatrix}I_{ion}(\mathbf{u}) & g(\mathbf{u})\end{bmatrix}^t$. Let $\pi_h \colon H^1(\Omega) \times L^2(\Omega) \longrightarrow S_h \times S_h$ be the projection and $\mathbf{u}_h = \begin{bmatrix}u_h & w_h\end{bmatrix}^t$ be the solution of the finite element formulation

$$(\mathbf{u}_{h,t}, \psi)_X + (DG\mathbf{u}_h, G\psi)_X = (\pi_h f(\mathbf{u}_h), \psi)_X, \forall \quad \psi \in S_h \times S_h. \tag{11}$$

**Theorem 1.** *Let* $\mathbf{u}$ *be the solution of the problem* (10)*, and* $\mathbf{u}_h$ *be the solution of the problem in semi-discrete case. Then, if* $I^{ion}(u,w)$ *and* $g(u,w)$ *is Lipschitz continuous in* $u$ *and* $w$ *and* $D(x)$ *is symmetric and positive definite, we have*

$$\| \mathbf{u}_h(T) - \mathbf{u}(T) \|_X \leq \| \mathbf{u}_{0,h} - \mathbf{u}_0 \|_X + Ch^2 \| \mathbf{u}_0 \|_X + Ch^2 \int_0^T (\| (F - \pi_h F)(\mathbf{u}) \|_X + \| \mathbf{u} \|_X + \| \mathbf{u}_t \|_X) dt. \tag{12}$$

Proof: Decompose the error

$$\mathbf{u} - \mathbf{u}_h = (\mathbf{u} - R_h\mathbf{u}) + (R_h\mathbf{u} - \mathbf{u}_h),$$

where $R_h\mathbf{u}$ is the elliptic projection of the $\mathbf{u}$ defined as,

$$(D(x)G(R_h\mathbf{u} - \mathbf{u}), G\chi)_X = 0, \quad \forall \quad \chi \in S_h \times S_h. \tag{13}$$

Now we will bound the $\theta = R_h\mathbf{u} - \mathbf{u}_h$ and $\rho = (\mathbf{u} - R_h\mathbf{u})$ separately.
In order to bound $\theta$, note that,

$$\begin{aligned}(\theta_t, \chi)_X + (D(x)G\theta, G\chi)_X &= -(\mathbf{u}_{h,t}, \chi)_X - (D(x)G\mathbf{u}_h, G\chi)_X + (R_h\mathbf{u}_t, \chi)_X + (D(x)GR_h\mathbf{u}, G\chi)_X, \\ &= -(\pi_h f(\mathbf{u}_h), \chi)_X + (R_h\mathbf{u}_t, \chi)_X + (D(x)G\mathbf{u}, G\chi)_X, \\ &= -(\pi_h f(\mathbf{u}_h)_X, \chi) + (f(\mathbf{u}), \chi)_X - (\mathbf{u}_t - R_h\mathbf{u}_t, \chi)_X,\end{aligned}$$

Therefore,

$$(\theta_t, \chi)_X + (D(x)G\theta, G\chi)_X = (f(\mathbf{u}) - \pi_h f(\mathbf{u}_h), \chi)_X - (\rho_t, \chi)_X.$$

Choose $\chi = \theta$, and applying Chauchy-Schwartz inequality in the above equation, we get

$$\begin{aligned}(\theta_t, \chi)_X + (D(x)G\theta, G\theta)_X &= (f(\mathbf{u}) - \pi_h f(\mathbf{u}_h), \theta)_X - (\rho_t, \theta)_X, \\ \frac{1}{2}\frac{d}{dt} \| \theta \|_X^2 + \alpha \| \nabla\theta \|_X^2 &\leq (\| f(\mathbf{u}) - \pi_h f(\mathbf{u}_h) \|_X + \| \rho_t \|_X) \| \theta \|_X .\end{aligned}$$

Since,$\| \nabla\theta \|_X^2 \geq 0$ and $\frac{d}{dt} \| \theta \|_X^2 = 2 \| \theta \|_X \frac{d}{dt} \| \theta \|_X$ . Therefore,

$$\begin{aligned}\frac{d}{dt} \| \theta \|_X &\leq \| f(\mathbf{u}) - \pi_h f(\mathbf{u}_h) \|_X + \| \rho_t \|_X, \\ &\leq \| f(\mathbf{u}) - \pi_h f(\mathbf{u}) \|_X + \| \pi_h f(\mathbf{u}) - \pi_h f(\mathbf{u}_h) \|_X + \| \rho_t \|_X .\end{aligned}$$

Now use that $f$ is Lipschitz continuous and the $L^2$ projection is bounded i.e. $\| \pi_h f(\mathbf{u}) \|_X \leq \| f(\mathbf{u}) \|_X$,

$$\frac{d}{dt} \| \theta \|_X \leq \| (f - \pi_h f)(\mathbf{u}) \|_X + M \| \mathbf{u} - \mathbf{u}_h \|_X + \| \rho_t \|_X .$$

After integration w.r.t. t from 0 to T we get,

$$\begin{aligned}\| \theta(T) \|_X &\leq \| \theta(0) \|_X + \int_0^T \| (f - \pi_h f)(\mathbf{u}) \|_X + M \| \mathbf{u} - \mathbf{u}_h \|_X + \| \rho_t \|_X \, dt, \\ \| \theta(T) \|_X &\leq \| \theta(0) \|_X + \int_0^T M(\| \theta \|_X + \| \rho \|_X) + \| (f - \pi_h f)(\mathbf{u}) \|_X + \| \rho_t \|_X \, dt.\end{aligned}$$

Now after applying Gronwall's lemma, we obtain,

$$\| \theta(T) \|_X \leq C(\| \theta(0) \|_X + \int_0^T \| \rho \|_X + \| (f - \pi_h f)(\mathbf{u}) \|_X + \| \rho_t \|_X \, dt).$$

Now, bounds for $\| \rho \|_X$ and $\| \rho_t \|_X$ we will take from the elliptic theory [13] which are given by,

$$\| \rho \|_X \leq Ch^2 \| \mathbf{u} \|_X,$$
$$\| \rho_t \|_X \leq Ch^2 \| \mathbf{u}_t \|_X .$$

Also,

$$\| \theta(0) \|_X \leq \| \mathbf{u}_{0,h} - \mathbf{u}_0 \|_X + \| R_h \mathbf{u}_0 - \mathbf{u}_0 \|_X \leq \| \mathbf{u}_{0,h} - \mathbf{u}_0 \|_X + Ch^2 \| \mathbf{u}_0 \|_X .$$

We arrive at the estimate,

$$\| \mathbf{u}_h(T) - \mathbf{u}(T) \|_X \leq \| \mathbf{u}_{0,h} - \mathbf{u}_0 \|_X + Ch^2 \| \mathbf{u}_0 \|_X + Ch^2 \int_0^T (\| (f - \pi_h f)(\mathbf{u}) \|_X + \| \mathbf{u} \|_X + \| \mathbf{u}_t \|_X) dt.$$

*3.1. Apriori error estimate for the fully discrete problem*

Let $k$ be the time step, $t_n = nk$, and let $U^n$ be the approximation of $\mathbf{u}(t_n)$ in $S_h \times S_h$. We will use backward Euler Galerkin scheme and linearize the equation (10) by replacing $U^n$ by $U^{n-1}$ to obtain

$$(\bar{\partial}_t U^n, \psi)_X + (D(x) G U^n, G\psi)_X = (F(U^{n-1}), \psi)_X, \quad \forall \quad \chi \in S_h. \tag{14}$$

Where, $\bar{\partial}_t U^n = \frac{1}{k}(U^n - U^{n-1})$.

**Theorem 2.** *Let $U^n$ and $\mathbf{u}$ be solutions of (14) and (6)-(8) respectively. Then, if $I^{ion}(u, w)$ and $g(u, w)$ are Lipschitz continuous in $u$ and $w$ and $D(x)$ is symmetric and uniformly positive definite, we have*
$\|U^n - \mathbf{u}(t_n)\|_X \leq C\|\mathbf{u}_{0,h} - \mathbf{u}_0\|_X + C(\mathbf{u})(h^2 + k) \forall t_n \in \bar{J}$.

**Proof.** $\mathbf{u}^n = \mathbf{u}(t_n)$ ,

$$U^n - \mathbf{u}^n = (U^n - \widetilde{U}^n) + (U^n - \mathbf{u}^n) = \theta^n + \rho^n, \tag{15}$$

where $\widetilde{U}^n$ is the elliptic projection of $\mathbf{u}^n$ defined as

$$(D(x) G(\widetilde{U}^n - \mathbf{u}^n), G\psi)_X = (DG\rho^n, G\psi)_X = 0, \tag{16}$$

$\rho^n$ will be bounded by Elliptic theory. Now we need to bound only $\theta^n$. For $\psi \in S_h \times S_h$,

$$\begin{aligned}
(\bar{\partial}_t \theta^n, \psi)_X + (D(x) G\theta^n, G\psi)_X =& ((\bar{\partial}_t U^n, \psi)_X + (D(x) G U^n, G\psi)_X - (\bar{\partial}_t \widetilde{U}^n, \psi)_X - (D(x) G\widetilde{U}^n, G\psi)_X \\
=& (F(U^{n-1}), \psi) - (\mathbf{u}_t^n, \psi)_X - (\overline{\partial_t} \tilde{U}^n - \mathbf{u}_t^n, \psi)_X - (D(x) G\tilde{U}^n, G\psi)_X \\
& - (D(x) G\mathbf{u}^n, G\psi)_X + (D(x) G\mathbf{u}^n, G\psi)_X, \\
=& (F(U^{n-1}), \psi)_X - (F(\mathbf{u}^n), \psi)_X - (\overline{\partial_t}(\tilde{U}^n - \mathbf{u}^n), \psi)_X \\
& - (D(x) G(\tilde{U}^n - \mathbf{u}^n), G\psi)_X - (\overline{\partial_t} \mathbf{u}^n - \mathbf{u}_t^n, \psi)_X.
\end{aligned}$$

Now using Lipschitz continuity of $F$,

$$\begin{aligned}
\| F(U^{n-1}) - F(\mathbf{u}^n) \|_X \leq C \| U^{n-1} - \mathbf{u}^n \|_X &\leq C(\| U^{n-1} - \mathbf{u}^{n-1} \|_X + \| \mathbf{u}^{n-1} - \mathbf{u}^n \|_X), \\
&\leq C(\| \theta^{n-1} \|_X + \| \rho \|_X + k \| \overline{\partial_t} \mathbf{u}^n \|_X).
\end{aligned} \tag{17}$$

Take $\psi = \theta^n$ and use the ellipticity of $D(x)$ and (17) we get,

$$\frac{1}{2}\overline{\partial_t}\| \theta^n \|_X^2 + \mu\| G\theta^n \|_X^2 \leq C(\| \theta^{n-1} \|_X + \| \rho^{n-1} \|_X + k \| \overline{\partial_t} u^n \|_X)(\| \theta^n \|_X) + (\| \overline{\partial_t}\rho^n \|_X + \| \overline{\partial_t}\mathbf{u}^n - \mathbf{u}_t^n \|_X) \| \theta^n \|_X .$$

Therefore,

$$\overline{\partial_t}\| \theta^n \|_X^2 \leq C(\| \theta^{n-1} \|_X^2 + \| \rho^{n-1} \|_X^2 + k\| \overline{\partial_t}\mathbf{u}^n \|_X^2) + \| \overline{\partial_t}\rho^n \|_X{}^2 + \| \overline{\partial_t}\mathbf{u}^n - \mathbf{u}_t^n \|_X{}^2 + C\| \theta^n \|_X{}^2$$
$$\overline{\partial_t}\| \theta^n \|_X^2 \leq C(\| \theta^n \|_X^2 + \| \theta^{n-1} \|_X^2 + T_h).$$

Using the Definition (3.1),

$$\| \theta^n \|_X{}^2(1 - Ck) \leq \| \theta^n \|_X^2(1 + Ck) + CkT_h$$

$$\| \theta^n \|_X^2 \leq \| \theta^n \|_X{}^2(1 + Ck)^2 + Ck(1 + Ck)T_h$$

$$\| \theta^n \|_X^2 \leq (1 + Ck)^{n+1}\| \theta^0 \|_X^2 + Ck\sum_{j=1}^{n}(1 + Ck)^{n-j+1}T_j$$

$$\| \theta^n \|_X^2 \leq C\| \theta^0 \|_X^2 + Ck\sum_{j=1}^{n} T_j$$

$$\| \rho^j \|_X = \| \tilde{U}^j - \mathbf{u}^j \|_X \leq Ch^2\| \mathbf{u}(jk) \|_X \leq C(\mathbf{u})h^2$$

$$\| \overline{\partial_t}\rho^j \|_X = \| k^{-1}\int_{(j-1)k}^{jk} \rho_t ds \|_X \leq C(\mathbf{u})h^2$$

$$\| \overline{\partial_t}\mathbf{u}^n - \mathbf{u}_t^n \|_X = \| k^{-1}\int_{(j-1)k}^{jk} (s - (j-1)k)\mathbf{u}_{tt}(s)ds \|_X \leq C(\mathbf{u})k.$$

We have $T_j \leq C(\mathbf{u})(h^2 + k)^2$.
Hence, $\| \theta^n \|_X \leq C \| \theta^0 \|_X + C(\mathbf{u})(h^2 + k)$.

## 4. Numerical Method

We consider the Monodomain model with ionic model. Variational formulation of the monodomain system is given as,

Given $u \in H^1(\Omega)$ and $w \in L^2(\Omega)$ (for FHN, Roger-McCulloch and Aliev-Panfilov) $w \in L^\infty(\Omega)$ (for Mitchell-Schaeffer) such that

$$C^m \int_\Omega \frac{\partial u}{\partial t}\zeta + \int_\Omega J(x)\nabla u \nabla \zeta + \int_\Omega I^{ion}(u, w)\zeta = 0, \tag{18}$$

$$\int_\Omega \frac{\partial w}{\partial t}\varsigma - \int_\Omega g(u, w)\varsigma = 0, \tag{19}$$

for all $\zeta \in H^1(\Omega), \varsigma \in L^2(\Omega)$.

Where, $H^1(\Omega) = \{u : u \in L^2(\Omega), \frac{\partial u}{\partial x_i} \in L^2(\Omega), i = 1, 2\}$ and
$L^2(\Omega) = \{u : \int_\Omega u^2 < \infty\}$ and $L^\infty(\Omega) = \{u : esssup \mid u \mid < \infty\}$

The system is discretized in space using finite element method and in time using Backward Euler method.

*4.1. Finite Element Discretization in Space*

We consider the square domain $\Omega = [a, b]^2$. Let $\tau_h$ be the partition of $\Omega$, into quasi-uniform grid of triangular linear elements $E$ such that $\Omega = \cup_{E \in \tau_h} E$.

The associated finite element space,

$V_h = \{\zeta_h \in H^1(\Omega) : \zeta_h$is continuous in$\Omega : \zeta_{h|E} \in P_1(E), \forall E \in \tau_h\}$,

where $P_1(E)$ =set of all linear polynomails in E and $\dim(V_h) = N$.

A semi-discrete form is obtained by applying a standard Galerkin procedure and choosing a finite element basis $\{\zeta_i\} \in V_h$. Let $I_h^{ion}$ be the finite element approximation of $I^{ion}$. Finite element approximation $u_h$ of transmembrane potential $u$ and $w_h$ of gating variable $w$ are given as

$u_h = \sum_{i=1}^{N} \alpha_i(t)\zeta_i$ and $w_h = \sum_{i=1}^{N} \beta_i(t)\zeta_i$ such that

$\frac{\partial u_h}{\partial t} = \sum_{i=1}^{N} \frac{\partial \alpha}{\partial t}\zeta_i$ and $\nabla u = \sum_{i=1}^{N} \alpha_i(t)\nabla\zeta_i$

where $\alpha = (\alpha_1, \alpha_2, ..., \alpha_N)$ and $\beta = (\beta_1, \beta_2, ..., \beta_N)$

Then the semidiscrete form is as follows,

$$C^m M \frac{\partial \alpha}{\partial t} + A\alpha + M I_h^{ion}(u_h, w_h) = 0, \tag{20}$$

$$\tag{21}$$

$$M \frac{\partial \beta}{\partial t} = MG(u_h, w_h), \tag{22}$$

where,

$M = (m_{jk}), m_{jk} = \sum_E \int_E \zeta_j \zeta_k dx,$

$A = (a_{jk}), a_{jk} = \sum_E \int_E \nabla {\zeta_j}^T J(x) \nabla \zeta_k dx.$

Numerical quadrature in 2-dimension is used in order to compute these integrals. Now this ODE system is discretized by Backward Euler and the nonlinear terms $I^{ion}$ and $G$ are linearized by taking values of $u_h$ and $w_h$ at the previous time step. The implementation is done using FreeFem++ library functions [8].

## 5. Numerical Results and Discussion

We consider the monodomain model with the following different ionic models (FHNM, RMM, APM, MSM) in a square domain $[-1.25, 1.25]^2$. We need to choose an appropriate grid system so that the numerical solution is computed upto an acceptable accuracy. Such a goal is achieved through the grid validation test. Three different grid systems consisting of (a) 991, (b) 1681 and (c) 2601 dofs have considered. We compare the action potential obtained using these grid systems. In all these cases only a marginal variation (less than 0.5%) in $v$ is found. As a sample grid validation test results related to monodoamin model with FHN and RM models provided in Fig.2. In both the cases, one can notice that there is not any variation in $u$ with increasing grid systems. Hence, all the computations have been carried out on $40 \times 40$ grid system.

*5.1. Computational Realization of $o(k + h^2)$*

We solved it using linear finite elements in space and Backward Euler in time and the nonlinear terms $I^{ion}$ and $g$ are linearized by taking values at the previous time step. We compute the $L^2$ norm of the error and the space and time rate of convergence. Initial conditions for $v$ and $w$ are chosen to be 0.2 , 0.1 respectively for all the cases and $I_{app} = 0, dt = h^2, Dx[n] = h, DT[n] = dt$. Space rate of convergence(sroc) = $log(L^2(e_{n-1})/L^2(e_n))/log(Dx[n-1])/Dx[n]$, time rate of convergence(troc) = $log(L^2(e_{n-1})/L^2(e_n)/log(DT[n-1])/DT[n]$, where $e_n : n^{th}$ level error.

From Tablel 1 it is clear that as the grid resolution is increased not only the error in $L^2$ norm decreases but also the theortically predicted sroc and troc are realized in all the cases.

| h | 1/8 | 1/16 | 1/32 | 1/64 | 1/128 |
|---|---|---|---|---|---|
| FHNM error | 0.0153718 | 0.00418786 | 0.0010467 | 0.000261422 | 6.53429e-05 |
| FHNM sroc | - | 1.876 | 2.00037 | 2.0014 | 2.00027 |
| FHNM troc | - | 0.937999 | 1.00018 | 1.0007 | 1.00014 |
| RMM error | 0.0293018 | 0.00587156 | 0.00132513 | 0.000321176 | 7.93853e-05 |
| RMM sroc | - | 2.31917 | 2.14761 | 2.04469 | 2.01642 |
| RMM troc | - | 1.15959 | 1.07381 | 1.02235 | 1.00821 |
| MSM error | 0.0123688 | 0.0030894 | 0.000772382 | 0.000193005 | 4.82713e-05 |
| MSM sroc | - | 2.00131 | 1.99994 | 2.0000 | 2 |
| MSM troc | - | 1.00065 | 0.999971 | 1.00004 | 0.999998 |
| APM error | 0.0110065 | 0.00273321 | 0.000681779 | 0.000170299 | 4.25639e-05 |
| APM sroc | - | 2.00969 | 2.00322 | 2.00123 | 2.000037 |
| APM troc | - | 1.00484 | 1.00161 | 1.00062 | 1.00018 |

Table 1: $L^2$ norm of the error and the space and time rates of convergence for different ionic models.

*5.2. Parametric Study Analysis*

It is to be noted that all the parameters in all the models considered under the current investigation are fixed to get physiological acceptance following the literature [7, 1, 5, 4]. However, there is freedom in varying the parameter $I_{app}$. Hence, the rest of the study is focused on exploring the effect of $I_{app}$ on different models. Numerical simulations are carried out in an implicit framework based on the backward Euler method with $dt = 0.001$.

Table 2: Parameter Values used for the Panfilov Model [1]

| $k$ | $\epsilon_0$ | $\mu_1$ | $\mu_2$ | $a$ |
|---|---|---|---|---|
| 8 | 0.2 | 0.2 | 0.3 | 0.15 |

Table 3: Parameter Values used for the Mitchell Schaeffer Model [5]

| $\tau_{in}$ | $\tau_{out}$ | $\tau_{open}$ | $\tau_{close}$ | $u_{gate}$ |
|---|---|---|---|---|
| 0.3 | 6 | 120 | 150 | 0.13 |

In order to understand the Cardiac Electrical Activity in a monodomain system with a class of ionic models, we start with the zero-dimensional (0-D) FHN ionic model and retrace the evolution of action potential ($v$) as reported in the literature [7]. The 0-D FHN ionic model [7] used in the simulation is stated below:

$$\epsilon \frac{du}{dt} = u(u - 0.1)(1 - u) - w + I_{app}, \tag{23}$$

$$\frac{dw}{dt} = u - 2w, \tag{24}$$

where the parameter $\epsilon = 0.01$ [7]. In Fig. 9 the time evolution of action potential ($u$) is traced for $u(0) = u_0 = 0.2, w(0) = w_0 = 0.2$, $dt = 0.001$ for $I_{app} = 0, 0.05, 0.15, 0.3, 0.65, 0.85$. The obtained result matches both qualitatively and quantitatively very well with those available in the literature for $I_{app} = 0, 0.15, 0.3$ [7]. Further, these plots depict the presence of $I_{app}$ sensitive stable and unstable equilibrium in the action potential. The periodic train pattern variation of action potential for $I_{app} = 0.05, 0.15$ Fig.(4-5) indicates the presence of an unstable equilibrium with a periodic limit cycle. Plots corresponding to $I_{app}$=0,0.3, 0.65, 0.85 depicts a stable equilibrium state in action potential. It is also to be noted from Fig.(3-8) that action potentials are initially for a very short time period get increasingly oscillatory with increasing $I_{app}$ prior to reaching a stable state. Our numerical experiments indicate that a choice of $I_{app} \in [0, 0.05) \cup (0.21, 0.85]$ will lead to a stable equilibrium and for $I_{app} \in [0.05, 0.21]$ will lead to periodic oscillations in an action potential.

Now we consider the 2-D monodomain system with the FHN ionic model as described below:

$$\epsilon\frac{du}{dt} - div(J(x)\nabla u) - u(u-0.1)(1-u) + w = I_{app} \qquad \text{in}[-1.25, 1.25]^2 \times (0,T), \tag{25}$$

$$\frac{dw}{dt} = u - 2w \qquad \text{in}[-1.25, 1.25]^2 \times (0,T), \tag{26}$$

with the homogeneous Neumann boundary condition in $v$.

Now, we numerically solve (25)-(26) by Galerkin Finite Element method in space and with backward Euler discretization in time with $dt = 0.001$ for $I_{app} \in [0, 0.85]$. The time evolution of action potential ($u$) is traced randomly at different $(x, y) \in [-1.25, 1.25]^2$ and found to be spatially uniform for all the points. In Fig. 16 the results corresponding to spatial coordiantes (0,0) (central point of domain) are presented. As in the 0-D case here again one can infer the manifestation of stable and unstable equilibrium with a periodic limit cycle as the $I_{app}$ is varied.

Next we repeat simulations with $u_0 = sin(x-0.5)+(y-0.1), w_0 = 0$ fixing $I_{app} = 0.15, 0.3$. The transmembrane potential contours corresponding these simulations at different time levels are presented in Fig.17 and Fig.18 respectively. From the iso-contour legend values one can notice an oscillatory nature of transmembrane potential when $I_{app} = 0.15$. However a stable behavior is observed when $I_{app} = 0.3$. Similar stable behavior is noticed for $I_{app} \in (0.2, 0.85]$.

Likewise, we numerically solve the 2-D monodomain system with Roger-McCulloch(RM), Panfilov, Mitchell-Schaeffer(MS) ionic models for different set of parameter values of $I_{app}$ by GFEM.

The monodomain system with RM ionic model is described below:

$$\epsilon\frac{du}{dt} - div(J(x)\nabla u) - u(u-0.1)(1-u) + uw = I_{app} \qquad \text{in} \quad [-1.25, 1.25]^2 \times (0,T),$$

$$\frac{dw}{dt} = u - w/2 \text{ in} \quad [-1.25, 1.25]^2 \times (0,T).$$

We trace the action potential for $I_{app} = [0, 0.85]$. In Fig.25 the action potential corresponding to (0,0) spatial coordiantes are presented. Action potential corresponding to the use of the RM ionic model is found to reach stable equilibrium for $I_{app} \in [0, 0.85)$. Results corresponding to $I_{app} = 0, 0.05, 0.15, 0.3, 0.65$ are presented in Fig.(19-24).

Now we consider RM model with $u_0 = sin(x-0.5)+(y-0.1), w_0 = 0$ fixing $I_{app} = 0.3$. The iso-transmembrane potential contours corresponding to these simulations at different time levels are presented in Fig.26. From the legend values one can notice that the solution depicts a stable behavior. Further the simulations are also repeated for $I_{app} \in [0.51, 0.85]$ with the modified initial data only to find that the solution always reaches to a stable state.

Action potential corresponding to the Panfilov ionic model is found to be unstable for all level set of $I_{app}$ with periodic limit cycle behavior. Unlike in other models the periods of these limit cycles are relatively very large and $\epsilon_0$ sensitive. Results pertaining to this model for different values of $I_{app}$ are presented in Fig.33.

Simulations corresponding to initial data $u_0 = sin(x-0.5)+(y-0.1), w_0 = 0$ with PF model carried out for different values of $I_{app}$. Results corresponding to $I_{app} = 0.3$ in the form of transmembrane potential contours are presented in Fig.34. These results depict a stable nature of the solution. The Solution remains stable despite changing $I_{app}$.

Now the results corresponding to the MS ionic model for different values of $I_{app}$ are presented in Fig.41. In all the cases action potentials are seen to reach a stable equilibrium state.

In Fig.42 iso-transmembrane plot contours corresponding to $I_{app} = 0.3$ for $u_0 = sin(x-0.5)+(y-0.1), w_0 = 0$ obtained from simulations based on MS model are presented. Clearly the solution is seen to reach a stable equilibrium. Further testing reveals that the stability is undisturbed by $I_{app}$.

## 6. Conclusions

Monodomain space-time 2-D cardiac tissue model in conjunction with different reduced cell-level models (FHNM, RM, APM, MSM) has been solved by FEM in space and backward Euler method in time. We compare the CEA triggered by these different reduced ionic models. Time evolution of transmembrane potential

corresponding to these models have been traced. Stability of the solution with each of these models is found to be sensitive to $I_{app}$. Under the given setting study reveals that RMM and MSM ionic models always leads to a stable solution, whereas the stability of APM is found to be highly sensitive to initial condition. $0-D$ FHN, $2D$ monodomain model with FHN and RM ionic model are found to have both stable and unstable zones of $I_{app}$. Also, For the Monodomain CEM in a generic framework for ionic models an apriori error estimate under fem approach has been theortically established and computationally verified.

**Acknowledgement**

We would like to thank to the DST for the support through Inspire Fellowship. Also thankful to FreeFem++ open source developers[9] for making it available for the researchers.

**References**

[1] Aliev R, Panfilov A, A simple two-variable model of cardiac excitation, *Chaos,solutions and Fractals* **7**:293-201, 1996.

[2] Nagumo JS, Arimoto S, Yoshizawa S, An active pulse transmission line stimulating nerve axon, *Proc. IRE*, pp. 2061-2071, 1962.

[3] Roger JM, McCulloch AD, A collocation-Galerkin finite element model of cardiac action potential propagation, *IEEE Trans. Biomed. Engr* **41(8)**:743-757, 1994.

[4] Franzone PC, Pavarino L, A parallel solver for reaction-diffusion systems in computational electrocardiology, *Math. Models Methods App* **14**:883-911, 2004.

[5] Mitchell CC, Schaeffer DG, A Two-Current Model for the Dynamics of Cardiac Membrane, *Bull. Math. Biol* **65(5)**:767-793, 2003 .

[6] Kunischa K, Wagner M, Optimal control of the bidomain system (I): The monodomain approximation with the Rogers–McCulloch model, *Nonlinear Analysis: Real World Applications* **13**:1525-1550, 2012.

[7] Franzone PC, Pavarino L, Scacch S, *Mathematical Cardiac Electrophysiology*, Springer, 2014.

[8] Hecht F, Pironneau O, Hyaric AL, Ohtsuka K, *FreeFem++ Manual*, Version 3.40, 2006.

[9] FreeFem++-cs an integrated environment for FreeFem++, http://www.freefem.org/ff++, 2014.

[10] Potse M, Dub́e B, Vinet A, Cardinal R, A comparison of monodomain and bidomain propagation models for the human heart, *EMBS Annual International Conference*, New York City, USA, 2006.

[11] Franzone PC, Pavarino L, Taccardi B, Simulating patterns of excitation, repolarization and action potential duration with cardiac Bidomain and Monodomain models, *Math. Biosci* **197(1)**:35-66, 2005.

[12] Smaill BH, LeGrice IJ, Hooks DA, Pullan AJ, Caldwell BJ, Hunter PJ, Cardiac structure and electrical activation: Models and measurement, *Clinical and Experimental Pharmacology and Physiology* **31**:913-919, 2004.

[13] V. Thomée, Galerkin Finite Element Methods for Parabolic Problems, Second ed., Springer-Verlag, 2006.

[14] Hasan IS, Paul DC, and Kwong TN, Three-Dimensional Finite-Difference Bidomain Modeling of Homogeneous Cardiac Tissue on a Data-Parallel Computer, *IEEE TRANSACTIONS ON BIOMEDICAL ENGINEERING* **44(2)**, 1997.

[15] Hanslien M, Karlsen KH, Tveito A, On a finite difference scheme for a Beeler-Reuter based model of cardiac electrical activity, *International Journal of Numerical analysis and Modeling* **3(4)**:395-412, 2006.

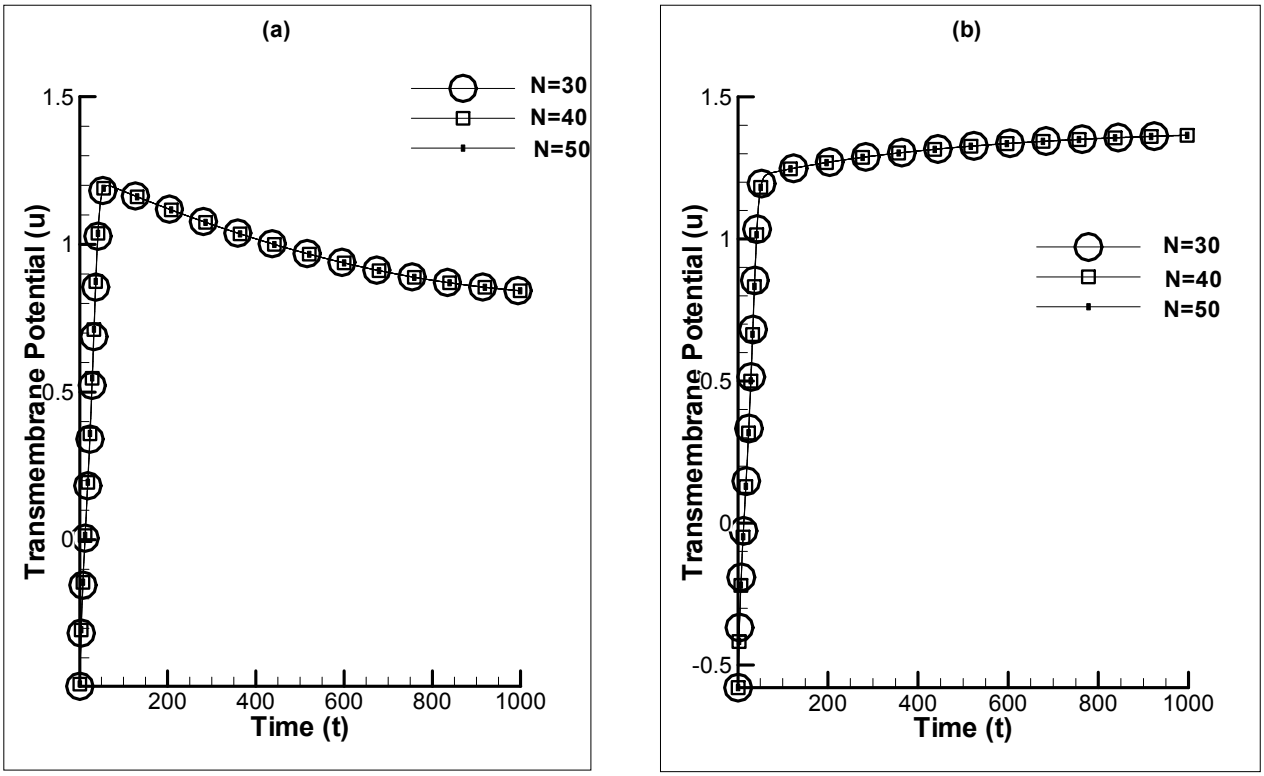


Figure 2: Grid Validation plot for Monodomain system with FHN (a) and RM (b) ionic models.

[t]0.5

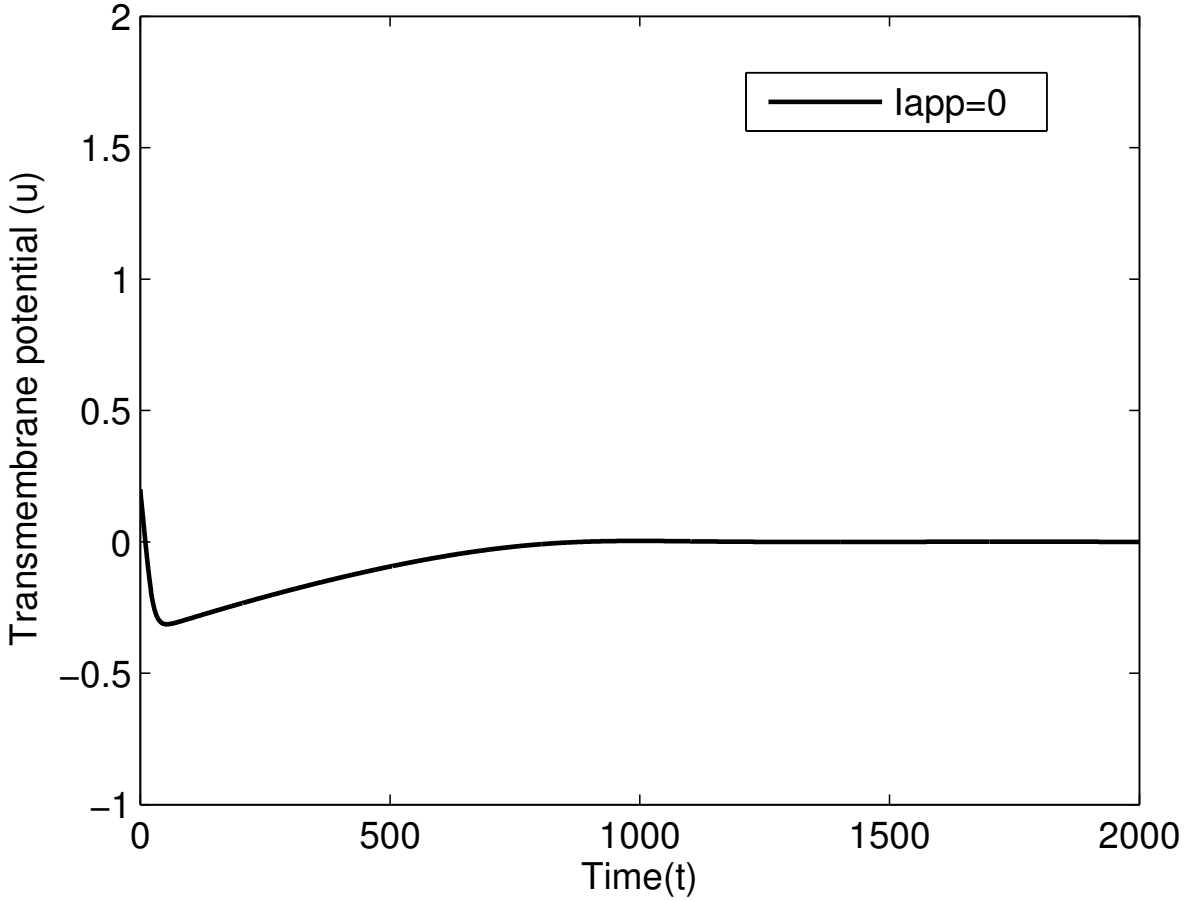


Figure 3

[t]0.5

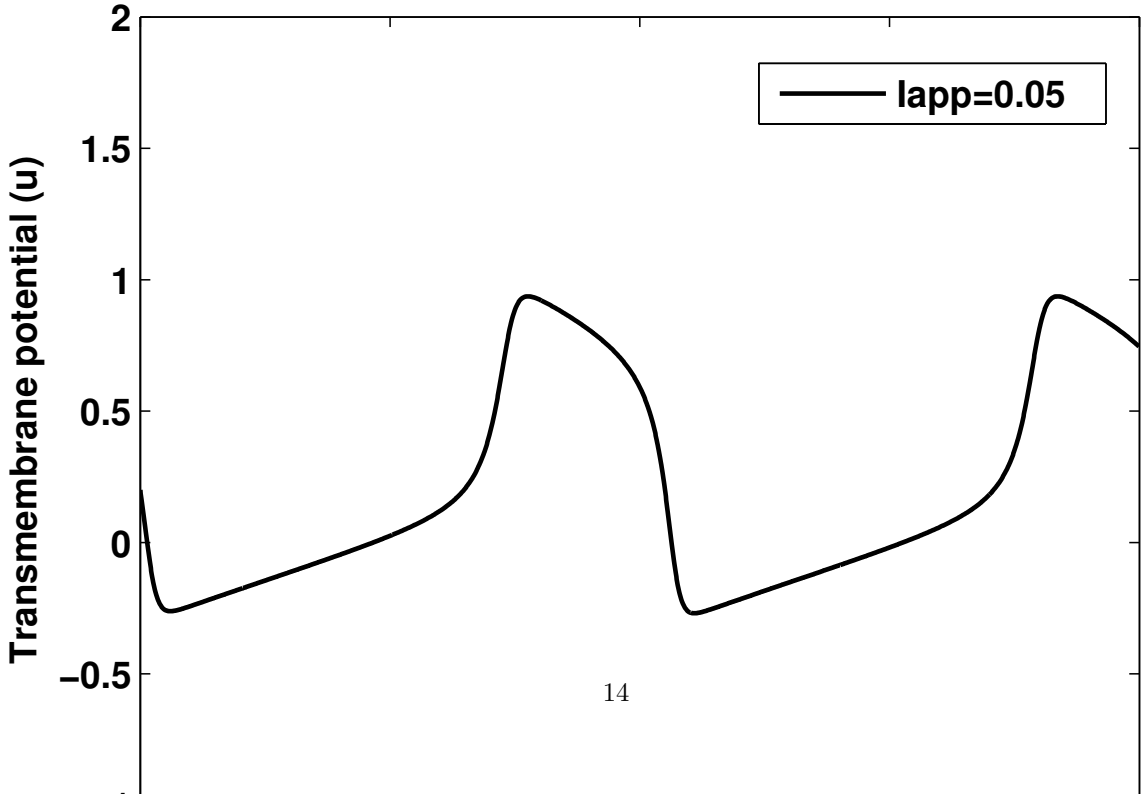

[t]0.5

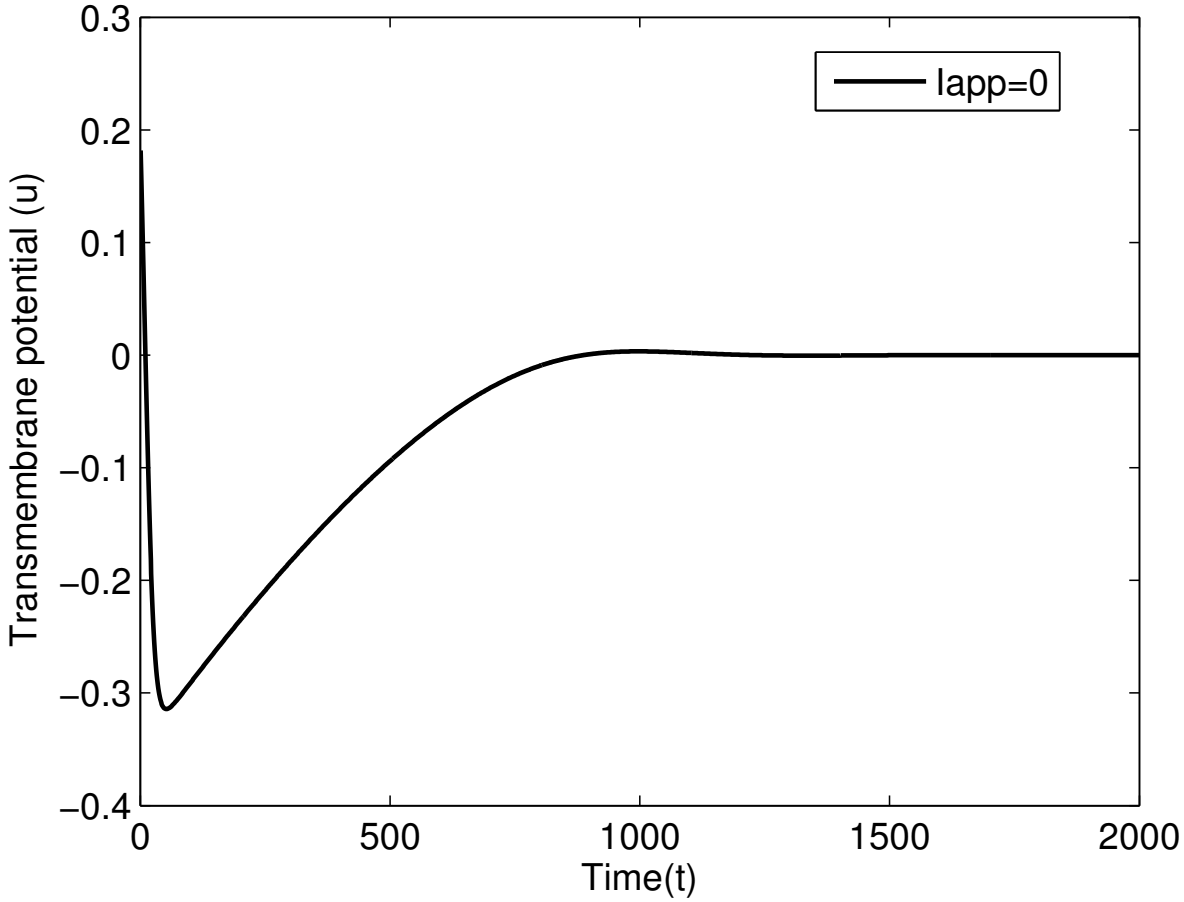


Figure 10

[t]0.5

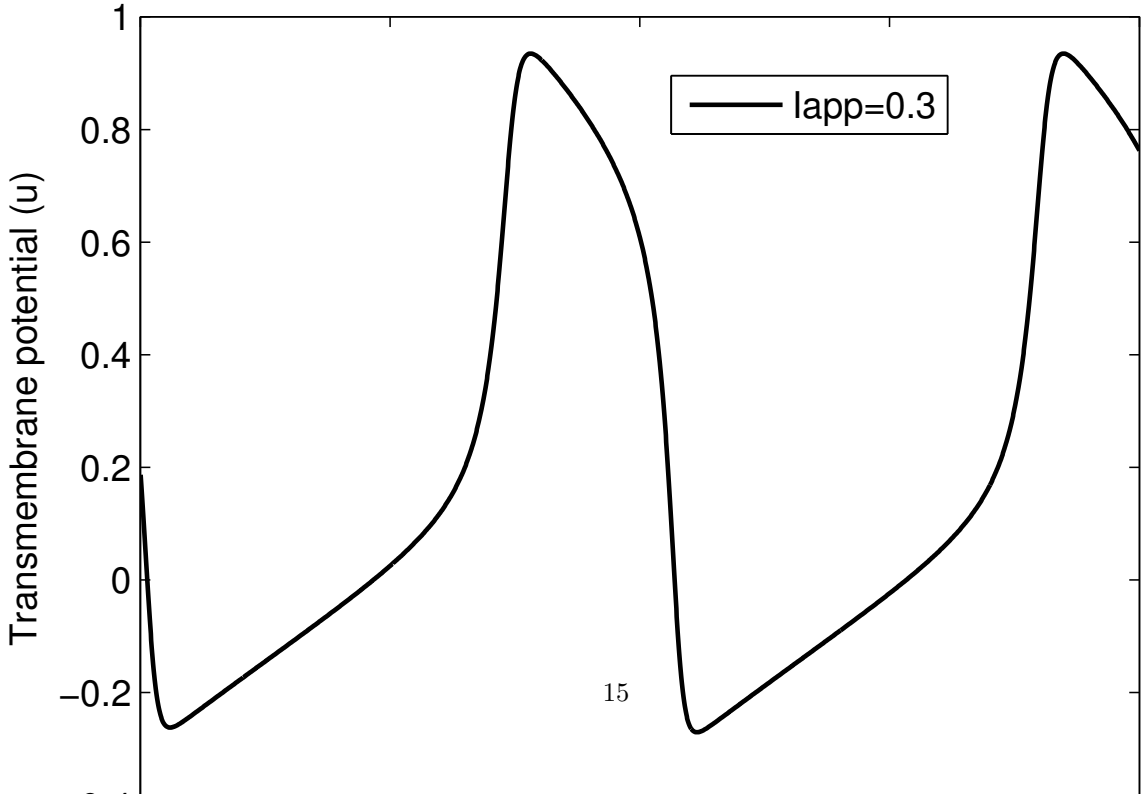

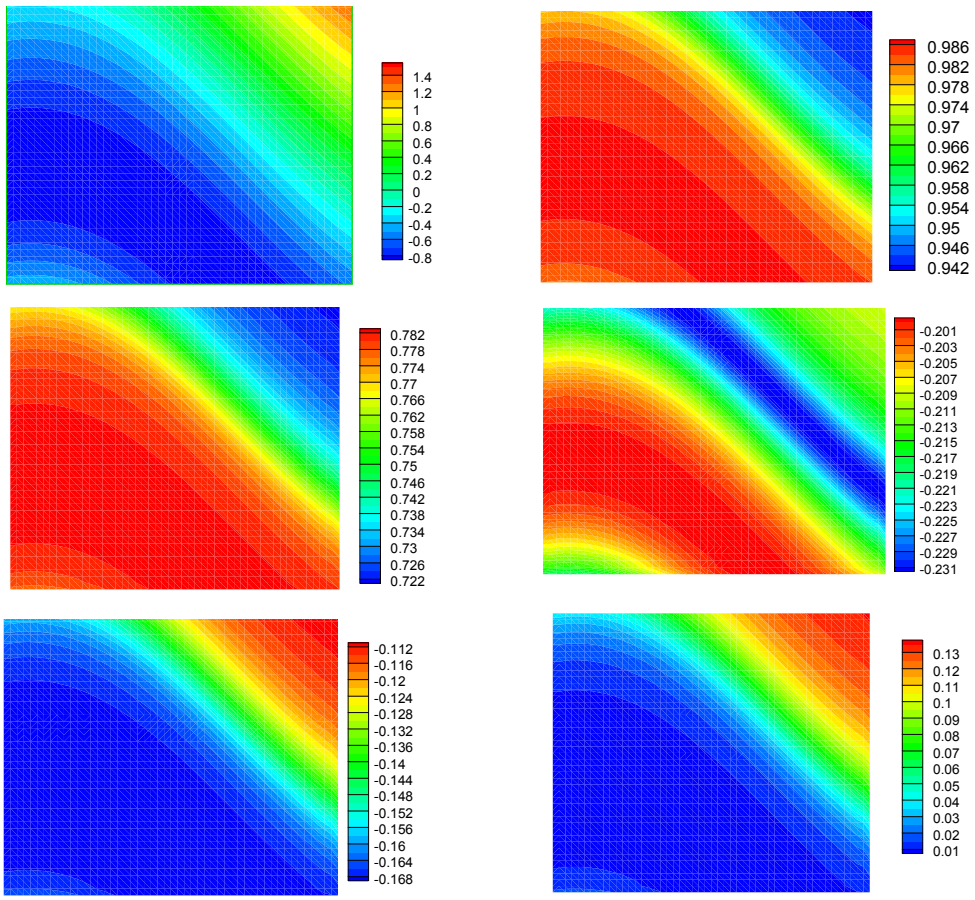


Figure 17: Iso-transmembrane potential contours for monodomain system with FHN ionic model when $I_{app} = 0.15$.

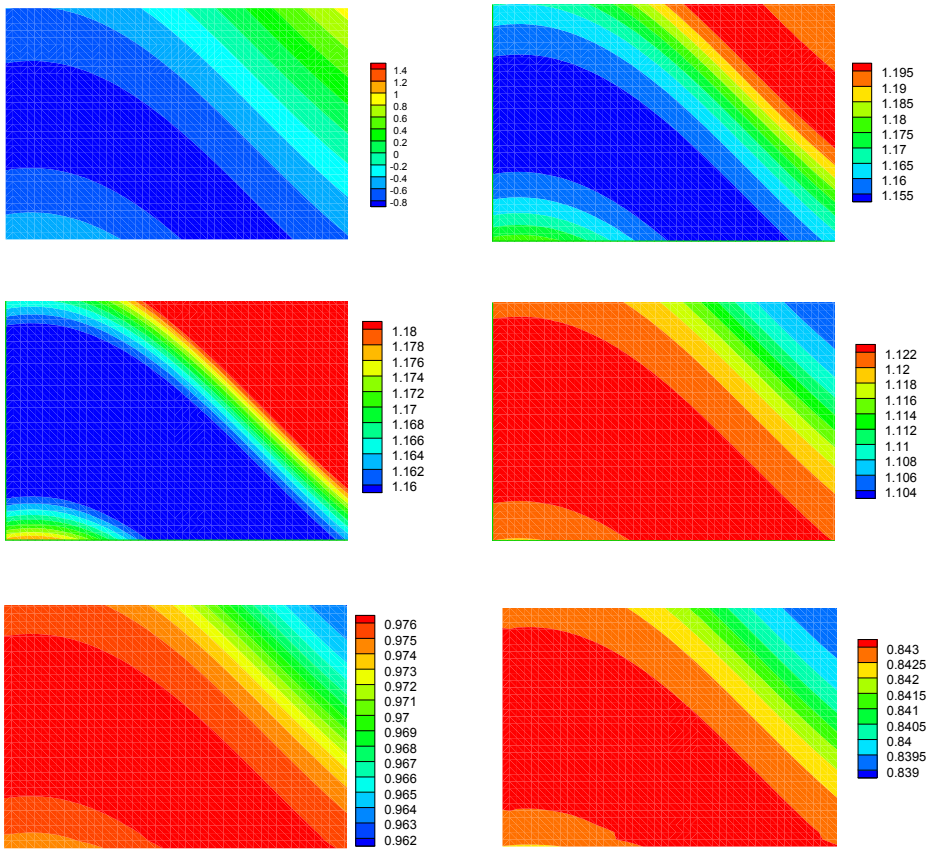


Figure 18: Iso-transmembrane potential contours for monodomain system with FHN ionic model when $I_{app} = 0.3$.

[t]0.5

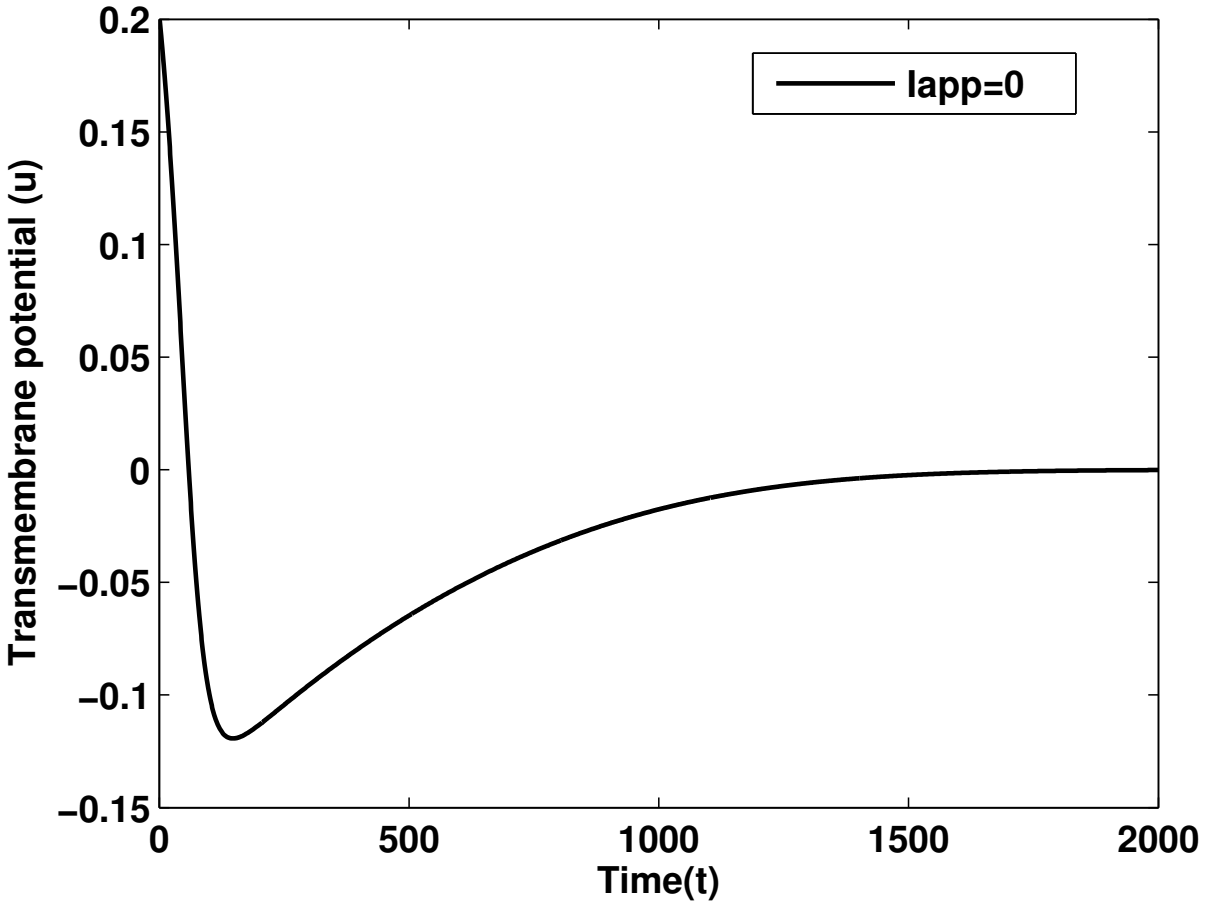


Figure 19

[t]0.5

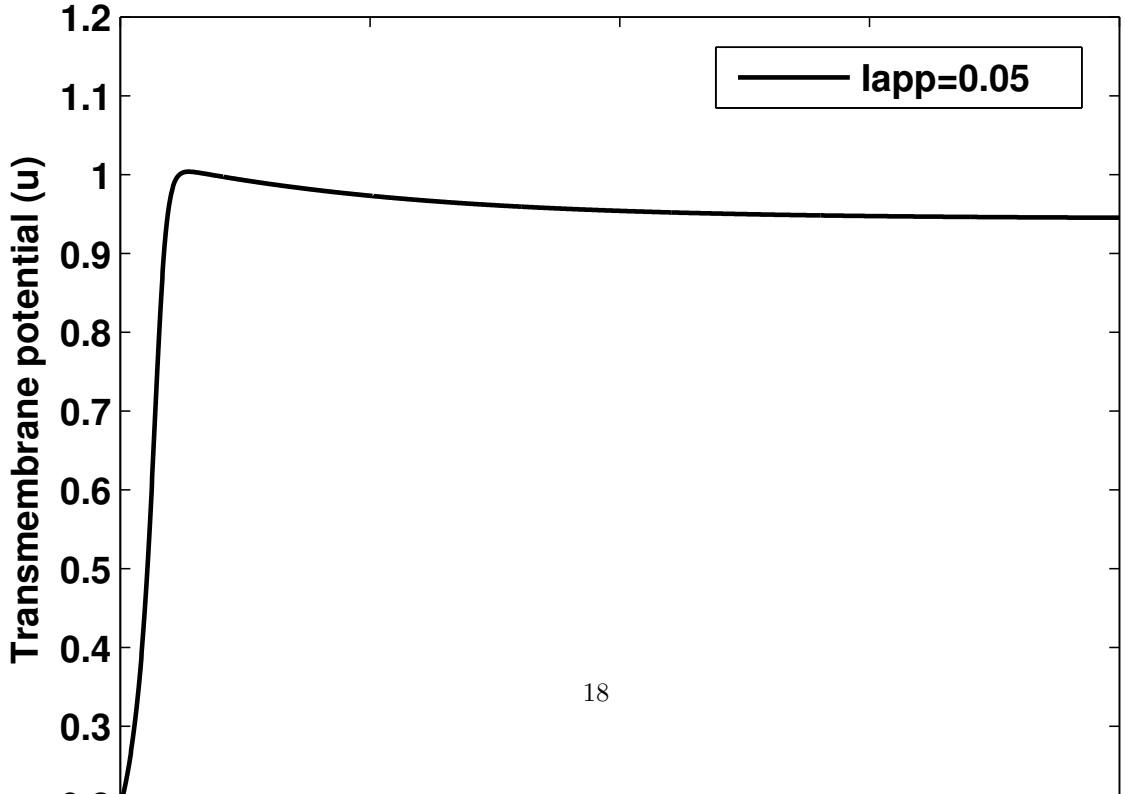

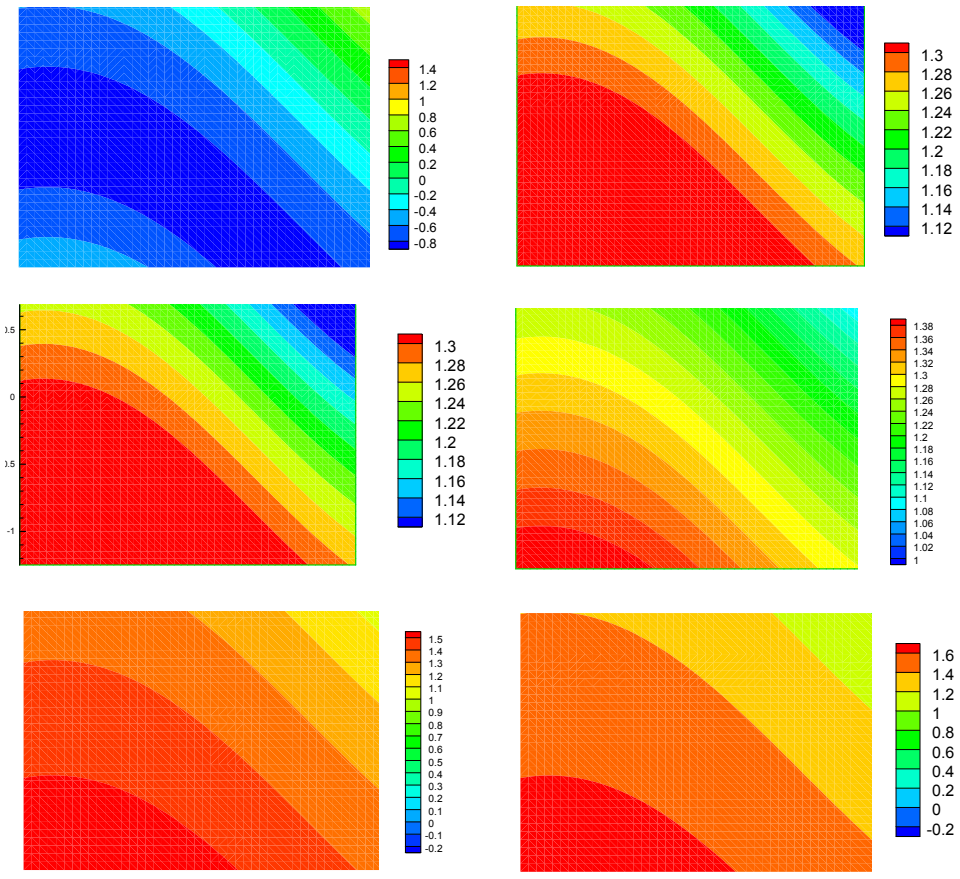


Figure 26: Iso-transmembrane potential contours for monodomain system with RM ionic model when $I_{app} = 0.3$.

[t]0.5

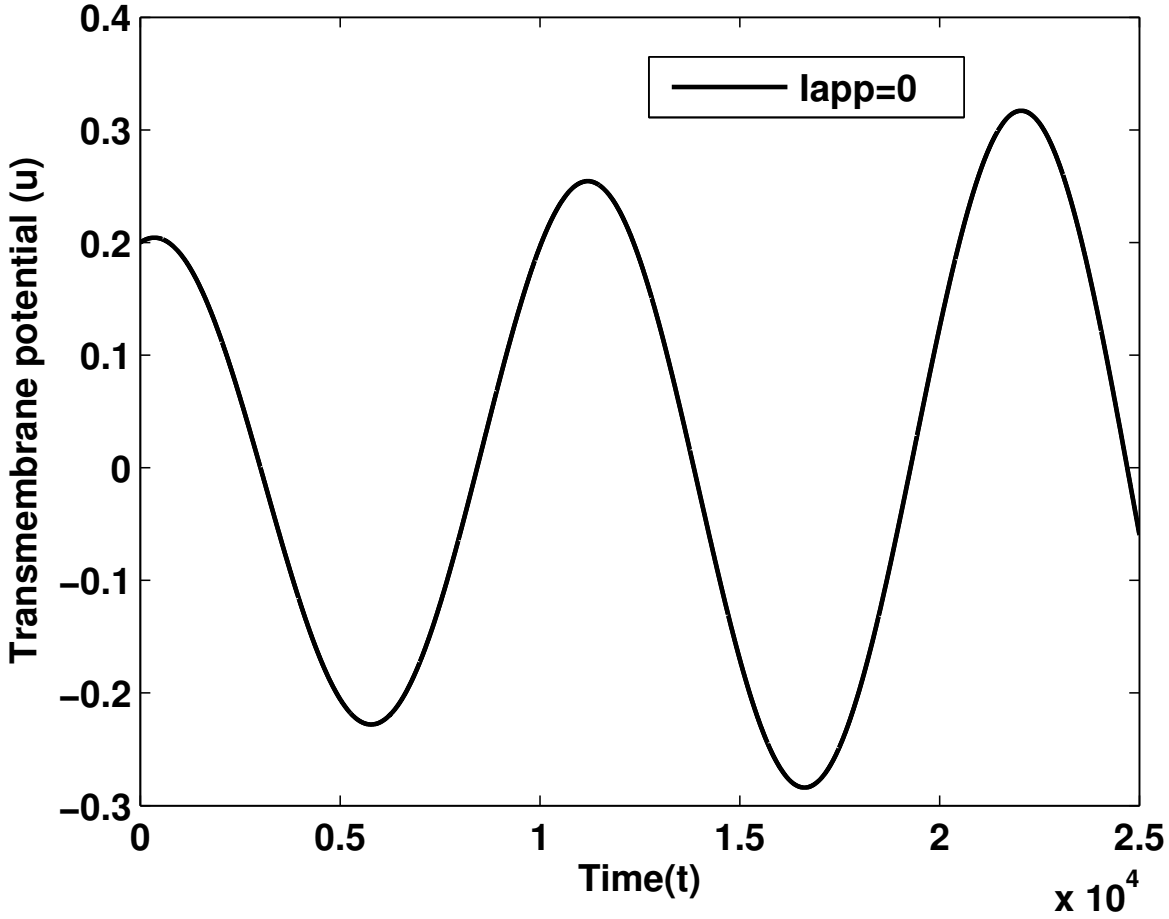


Figure 27

[t]0.5

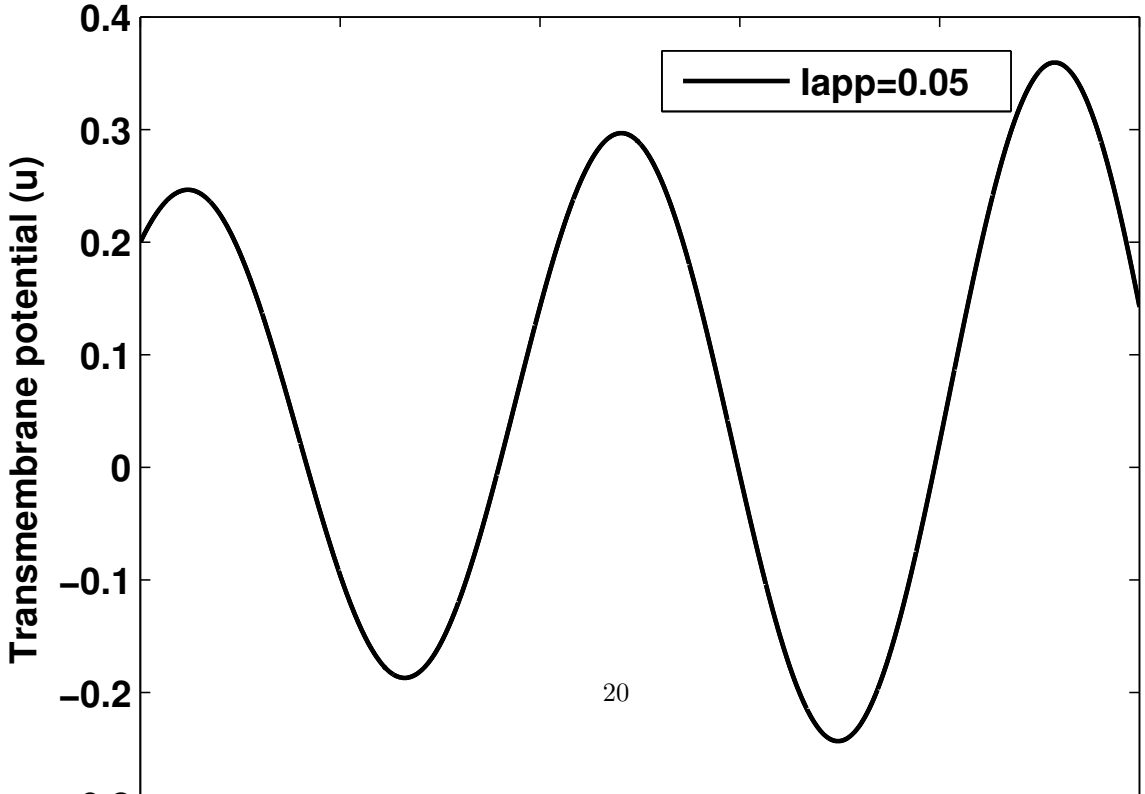

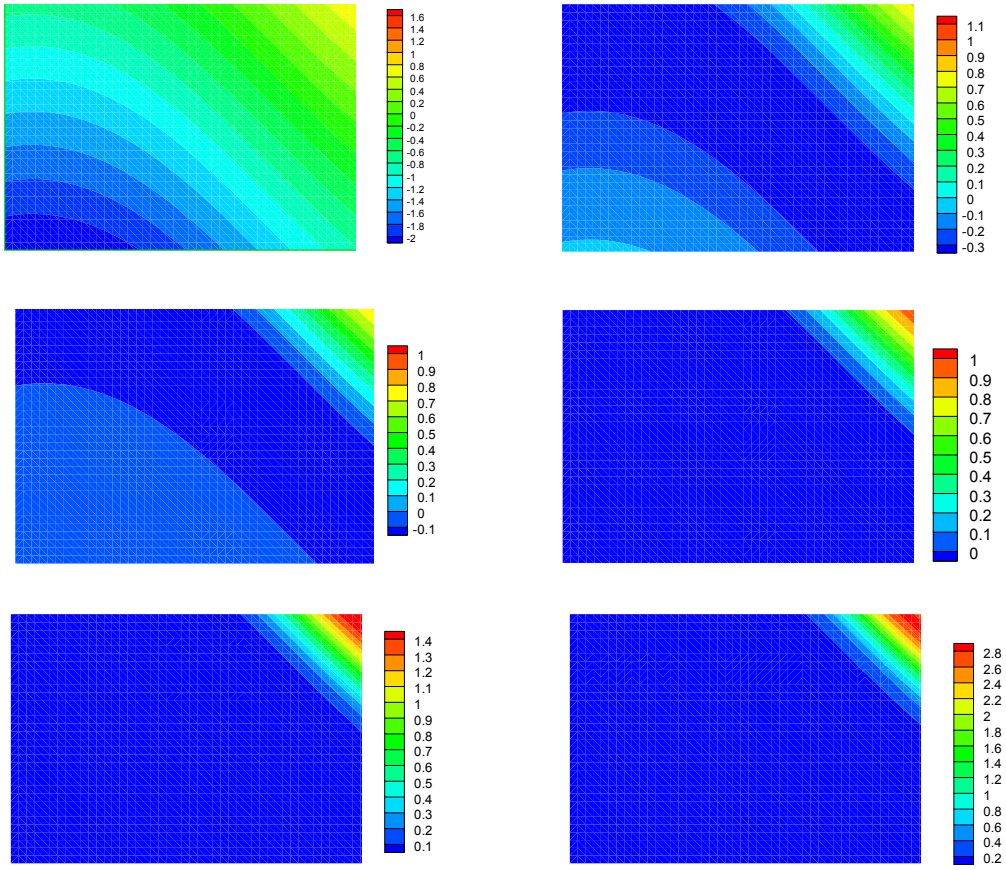


Figure 34: Iso-transmembrane potential contours for monodomain system with Panfilov ionic model when $I_{app} = 0.3$.

[t]0.5

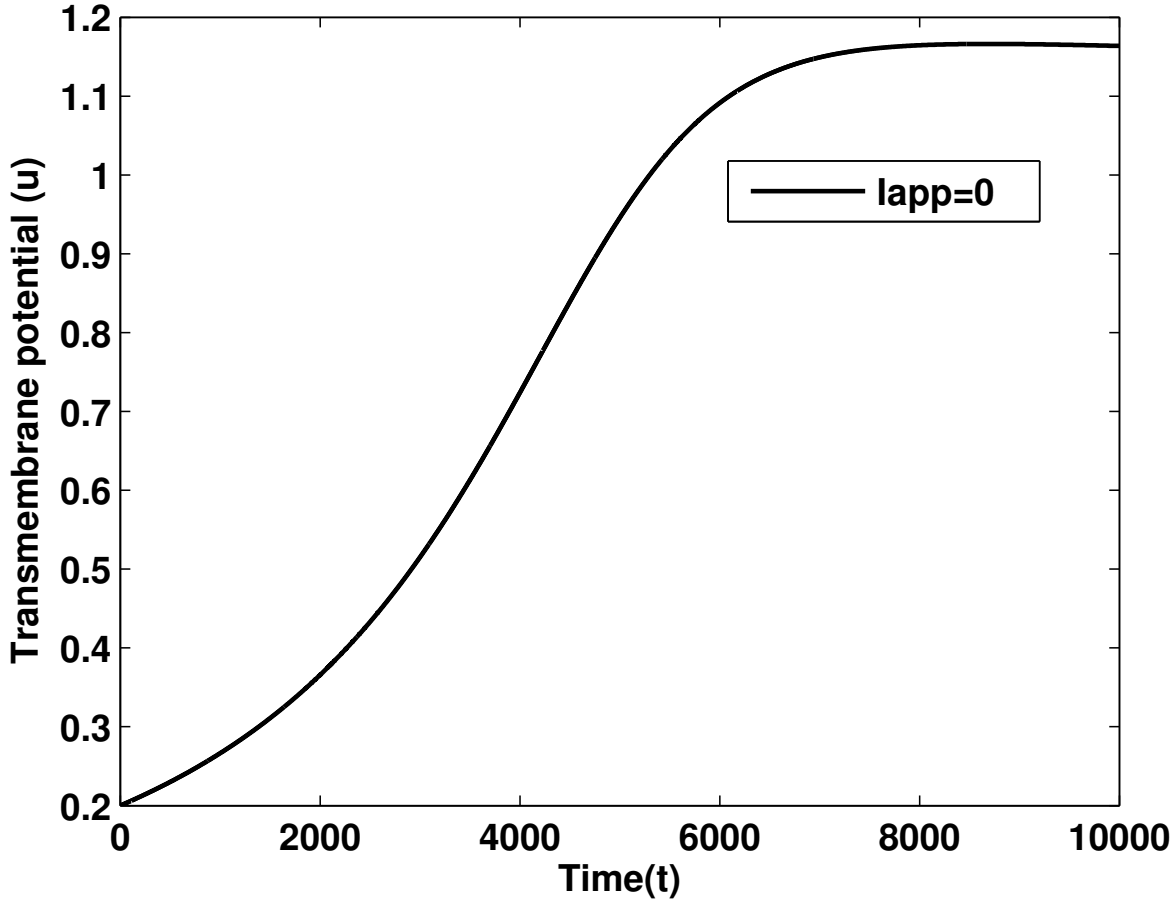


Figure 35

[t]0.5

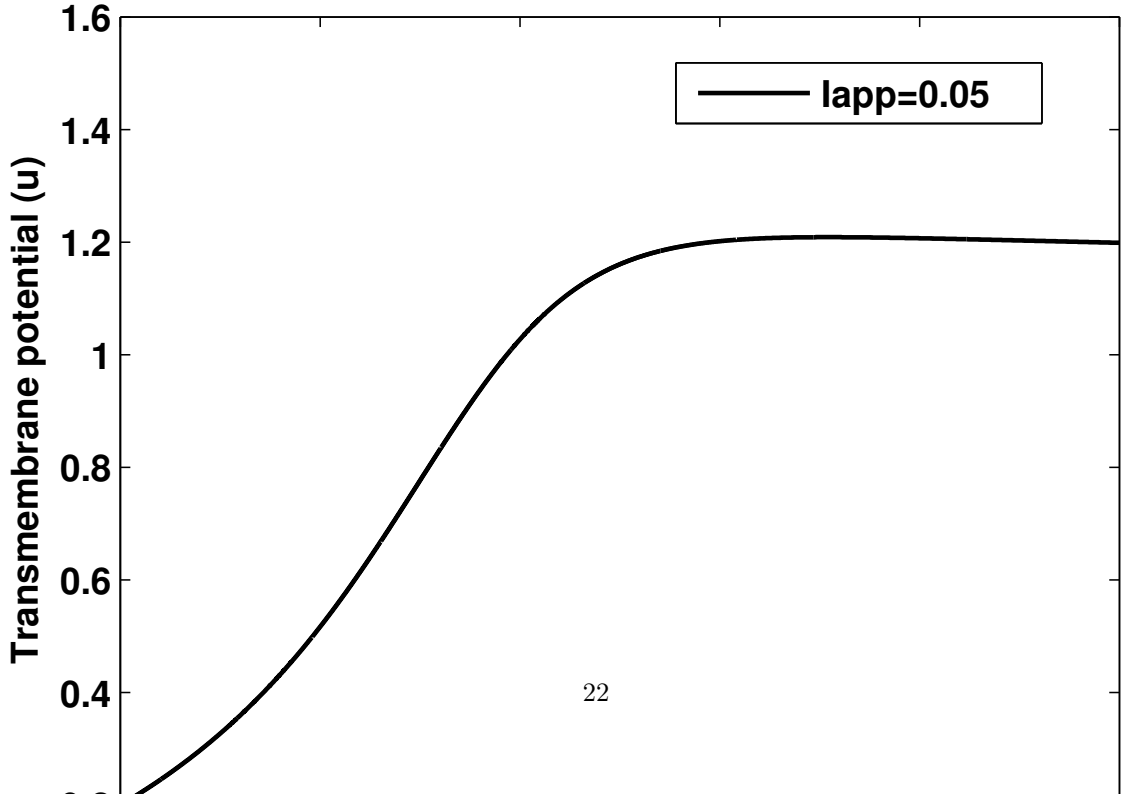

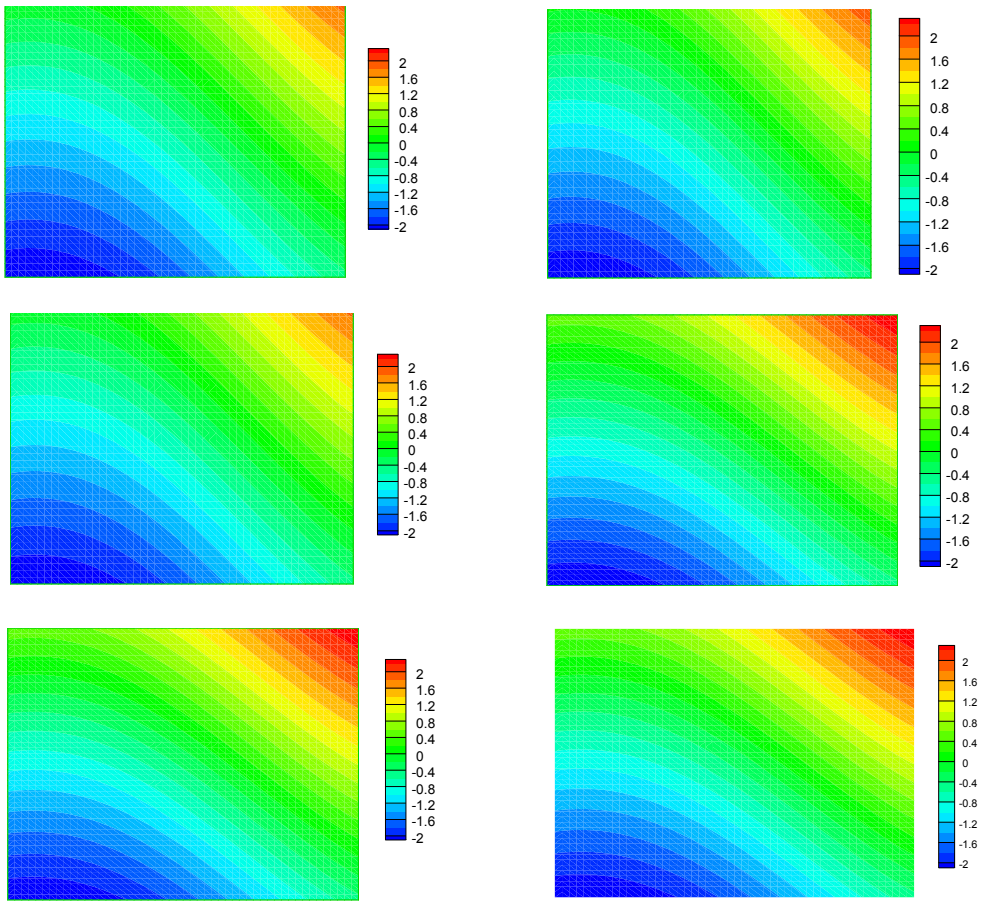


Figure 42: Iso-transmembrane potential contours for monodomain system with MS ionic model when $I_{app} = 0.3$.